

Supplement of *Clim. Past Discuss.*, 11, 2483–2555, 2015
<http://www.clim-past-discuss.net/11/2483/2015/>
doi:10.5194/cpd-11-2483-2015-supplement
© Author(s) 2015. CC Attribution 3.0 License.



Supplement of

Continental-scale temperature variability in PMIP3 simulations and PAGES 2k regional temperature reconstructions over the past millennium

Correspondence to: H. Goosse (hugues.goosse@uclouvain.be)

The copyright of individual parts of the supplement might differ from the CC-BY 3.0 licence.

1 *Sect. S1: processing of the model time series and instrumental data*

2 Model data were processed to correspond to the temporal and area-weighted spatial
3 averaging of the PAGES 2k temperature reconstructions (PAGES 2k Consortium, 2013) for
4 each region as follows:

- 5 1. Antarctica (annual): 90° S-60° S ; 180° W-180° E
- 6 2. Arctic (annual): 60° N-90° N ; 180° W-180° E
- 7 3. Asia (June-August): 23.5° N-55° N ; 60° E-160° E
- 8 4. Australasia (September-February): 50° S-0° S ; 110° E-180° E
- 9 5. Europe (June-August): 35° N:70° N ; 10° W-40° E
- 10 6. North America (annual)*: 30° N:55° N ; 130° W-75° W
- 11 7. South America (December-February): 65° S-20° S ; 75° W-30° W

12 Note that all simulations for North America were bilinearly interpolated to the
13 HadCRUT3V latitude-longitude grid before the grid box centred at 52.5° N; 77.5° W was
14 removed from the averaging calculation to match processing of the instrumental predictand
15 (PAGES 2k Consortium, 2013).

16 The ocean was masked for Antarctica, Asia, Europe and South America regions using
17 the respective binary (1, 0) land masks for each simulation. No significant difference was
18 found between the use of fractional land masking (proportion between and including 0 and 1)
19 and the binary mask common to all simulations for the land-only PAGES 2k reconstruction
20 equivalent.

21 As the GISS-E2-R control simulation is known to contain a drift from non-equilibrated
22 initial conditions (Schmidt et al., 2014), the transient as well as the control simulation from
23 that model have been detrended by subtracting a low-frequency loess fit that has been
24 estimated from the corresponding time period of the control simulation from each time series.

25 The statistical framework by Sundberg et al. (2012), used in sections 3.4 and 6.2,
26 requires that all proxy-based temperature reconstruction time series are re-calibrated to suit
27 certain assumptions. To this end, gridded instrumental temperature data were used and
28 averaged over exactly the same regions and seasons as explained above for the models. To
29 comply with the different boundaries and land/sea masks used, the respective instrumental
30 series were derived from CRUTEM4 (Jones et al., 2012) for regions 5 and 6, HadCRUT4
31 (Morice et al., 2012) for regions 2, 4 and 6 and CRU TS3 (Harris et al., 2014; as updated and
32 available on the KNMI Climate Explorer, <http://climexp.knmi.nl/>, on April 23, 2014) for
33 region 3. For region 1, we used the same instrumental target series as the PAGES 2k
34 Consortium (2013). Re-calibration was made for the same calibration periods as used by the
35 PAGES 2k Consortium. Each instrumental target series was arbitrarily assumed to contain
36 10% noise variance. Sensitivity experiments were also made with assumptions of 5% and
37 15% noise. This had no effect on any main conclusions.

38

39 *Sect. S2: estimate of the forcing used in the superposed epoch analysis*

40 The Crowley and Untermann (2012) volcanic forcing reconstruction is provided in
41 aerosol optical depth (AOD) distributed into four equal-area latitudinal bands (-30°S, 0-30°S,
42 0-30°N, 30-90°N). The original data are translated to W/m² through multiplying by -20
43 (Wigley et al., 2005). The volcanic forcing for each region is subsequently selected by
44 identifying the corresponding latitudinal band or by constructing a weighted average based on
45 the relative proportions of the regional area if two latitudinal bands are involved. In the case

46 of the Gao et al. (2008) reconstruction, 18 latitudinal bands of 10° are considered as well as a
47 vertical distribution of aerosols discretized into 43 levels. A total integral of the aerosol
48 loading in the vertical dimension is first obtained for each latitudinal band and time step. An
49 average of the loadings of the various latitudinal bands that constitute each region is
50 subsequently calculated. The original loadings (kg/km^2) are converted into AOD by first
51 multiplying by the area of the Earth in km^2 and dividing by 150 Tg (Stothers et al., 1984) after
52 converting kg to Tg. The resulting AOD are then converted into W/m^2 by a factor of -20
53 following Wigley et al. (2005) as in the previous case.

54

55 *Sect. S3: correlation between simulated and reconstructed time series.*

56 Figure S1 displays the correlation between the 23-year Hamming filtered model
57 simulation results and temperature reconstructions for individual regions. This illustrates the
58 agreement between the contribution of radiative forcing on observed temperatures and in the
59 model simulations. The highest correlation values are obtained for the Arctic region in most
60 simulations (Figure S1a). Correlations for the North American pollen-based reconstruction
61 and for Australasia and Europe tend to be highly significant. Correlations tend to be non-
62 significant for the North American tree reconstruction, and for the South American and
63 Antarctic reconstructions.

64 If we consider the available single-model ensembles (Figure S1b; COSMOS and GISS),
65 the correlation of the ensemble mean with the regional temperature reconstructions is always
66 higher than the average of all individual member correlations. The ensemble averaging
67 reduces the internal variability present in the simulated series in favour of the response to the
68 external forcing common in simulation results and reconstructed temperature.

69

70 *Sect. S4: EOF analysis for GISS and COSMOS ensembles.*

71 Investigating the variability in the GISS and the COSMOS ensemble simulations
72 provides insights into the intra-model spread. The (detrended) GISS simulations show a very
73 coherent picture with similar loadings and variance explained by the leading EOF (~80-90 %)
74 for the different regions within the single ensemble members (Fig. S7). However, the
75 COSMOS simulations have a larger spread of the variance explained by the leading EOF. The
76 larger heterogeneity in the COSMOS simulations might be indicative of a larger amount of
77 internal variability and hence less externally forced spatial coherence among the regions. For
78 the ensemble with the larger scaling of the solar forcing (COSMOSe2, Fig. S7) the amount of
79 variance represented by the leading EOF is larger compared to the weaker scaling
80 (COSMOSe1, Fig. S7), indicating a larger common forced signal in the different ensemble
81 members.

82

83 *Sect. S5: correlation between hemispheres.*

84 An analysis of coherence between hemispheric temperatures, calculated herein simply
85 by weighting the individual regions according to their area (Fig. S10), confirms the results of
86 Neukom et al. (2014) in the sense that the two hemispheres are significantly correlated during
87 most of the last millennium in model simulations. The control simulations indicate a natural

88 tendency for inter-hemispheric correlation in models. Nevertheless, the correlation during
89 periods with strong external forcing clearly exceeds the range derived from control
90 simulations (not shown). In the reconstructions, the Southern Hemisphere experienced
91 temperature anomalies opposite to the ones in the Northern Hemisphere during long periods
92 of the first half of the millennium, indicative of non-coherence between the two hemispheres
93 and potentially unforced variability.

94

95 *Sect. S6: superposed epoch analysis for the Gao et al. (2008) forcing.*

96 The reconstruction of volcanic forcing by Gao et al. (2008) provides larger estimates
97 than Crowley and Unterman (2012) and with more inter-regional differences (Fig. S11). The
98 largest forcing composites are in Australasia, Asia, South America and Europe with values
99 between -10 and -5 Wm⁻². The simulated response is homogeneous among regions, with
100 simulated changes of the order of -1 to -0.5 °C. The reconstructed temperature response is
101 again weaker than the simulated one, with particularly negligible signal for Australia and
102 Antarctica.

103

104 Additional references

105 Harris, I., Jones, P.D., Osborn, T.J., and Lister, D.H: Updated high-resolution grids of
106 monthly climatic observations – the CRU TS3.10 Dataset, *Int. J. Climatol.*, 34, 623-642,
107 doi:10.1002/joc.3711. 2014

108 Jolliffe, I. T. and Primo, C.: Evaluating rank histograms using decompositions of the
109 chi-square test statistic, *Mon. Weather Rev.*, 136, 2133–2139, doi: 10.1175/2007MWR2219.1,
110 2008.

111 Jones, P. D., Lister, D. H., Osborn, T. J., Harpham, C., Salmon, M., and Morice, C. P.,
112 Hemispheric and large-scale land surface air temperature variations: An extensive revision
113 and an update to 2010, *J. Geophys. Res.*, 117, D05127, doi:10.1029/2011JD017139, 2012

114 Priestley, M. B. *Spectral analysis and time series*, Academic Press, 1982.

115

116

117

118 **Supplementary table S1: additional information on model simulation sources**

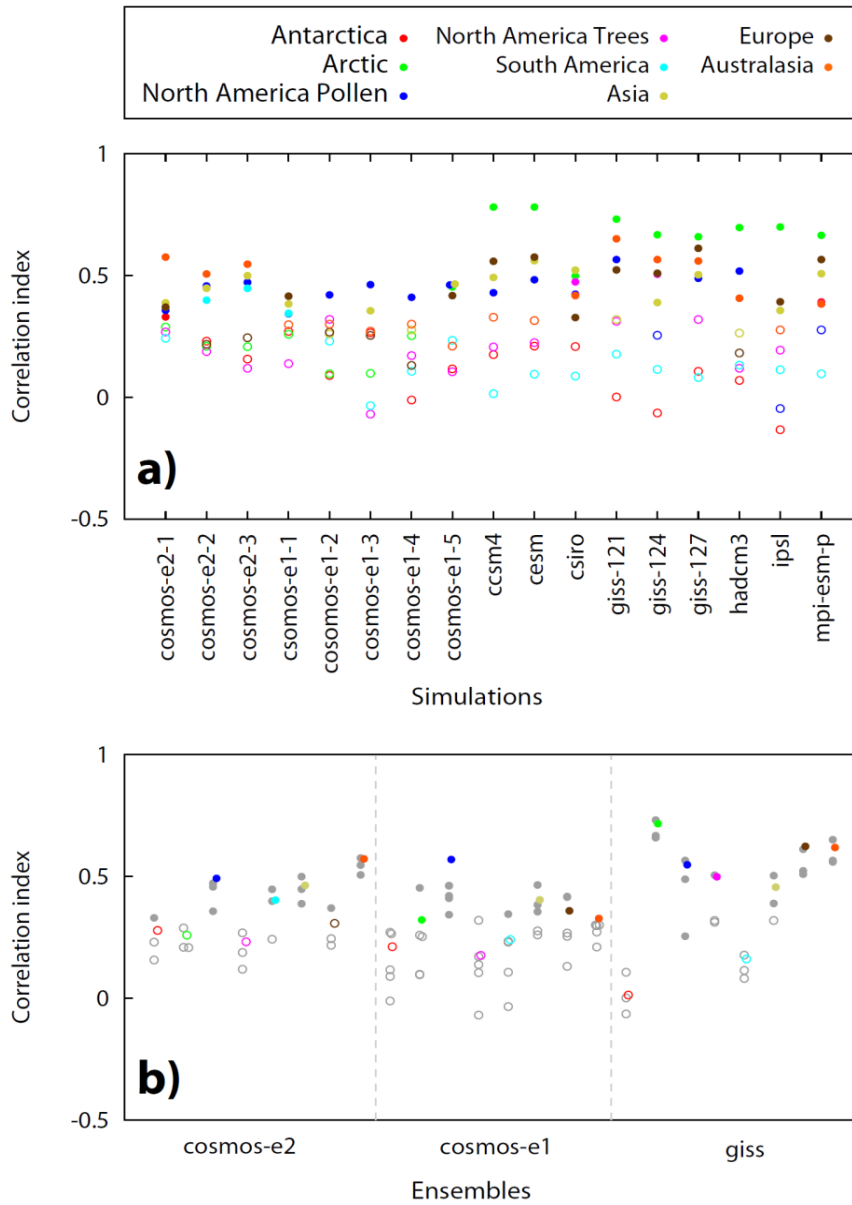
Model	past1000	historical extension	Source past1000	Source historical extension	Reference
CCSM4	r1i1p1	r1i2p2	PMIP3 ¹	PMIP3	Landrum et al. (2013)
CESM1	Single continuous simulation (not contained in the CMIP5/PMIP3 database)		Flavio Lehner (lehner@climate.unibe.ch)	Flavio Lehner (lehner@climate.unibe.ch)	Lehner et al. (submitted.)
CSIRO-Mk3L-1-2	r1i1p1	r1i1p1	PMIP3	PMIP3	Phipps et al. (2013)
GISS-E2-R	r1i1p12[1,4,7]	r1i1p12[1,4,7]	PMIP3	PMIP3	Schmidt et al. (2013)
HadCM3	r1i1p1	exists, but is not in CMIP5/PMIP3 database	PMIP3 ²	Andrew Schurer (aschurer@staffmail.ed.ac.uk)	Schurer et al. (2013)
IPSL-CM5A-LR	r1i1p1	exists, but is not in CMIP5/PMIP3 database	PMIP3	PMIP3	Dufresne et al. (2013)
MPI-ESM-P	r1i1p1	r1i1p1	PMIP3	PMIP3	Jungclaus et al. (2014)
ECHAM5/MPIOM	continuous simulations (pre-PMIP3, no rip code)		CERA ³	CERA	Jungclaus et al. (2010)

119

120 ¹ <http://pcmdi9.llnl.gov/esgf-web-fe>121 ² <http://badc.nerc.ac.uk/browse/badc/euroclim500/data/ALL/r1>122 ³ <http://cera-www.dkrz.de/CERA>

123

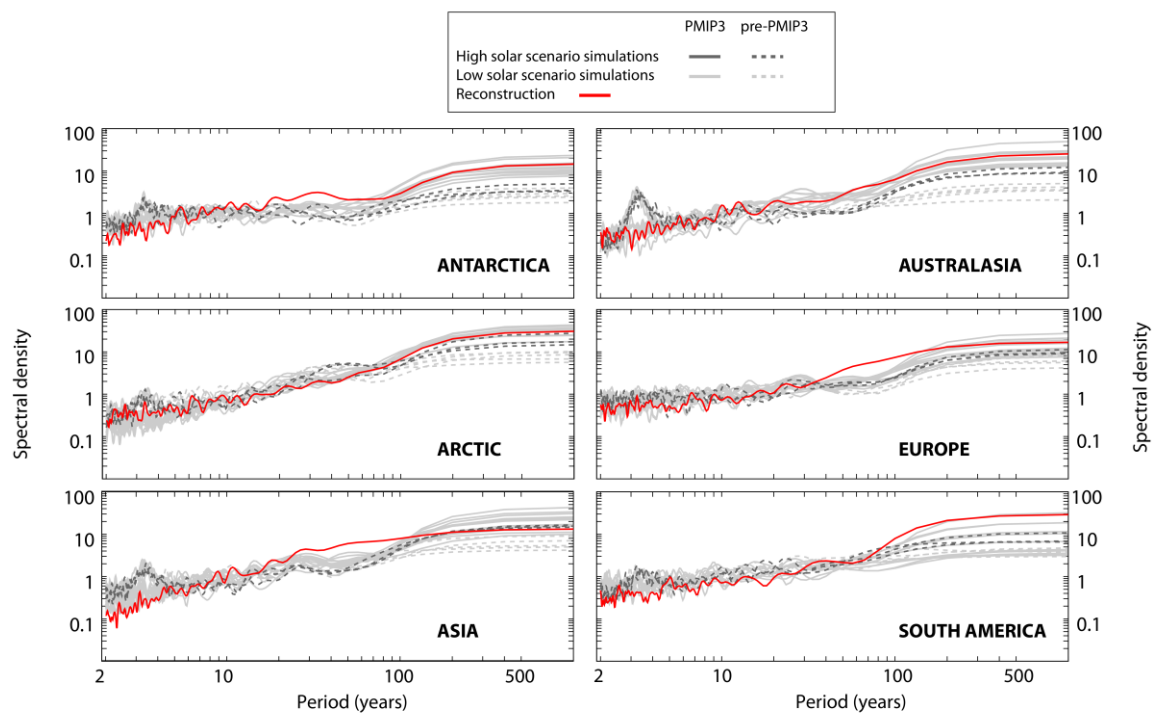
124



125

126 Figure S1. a) Correlations between 23-year Hamming filtered PAGES 2k temperature
 127 reconstructions and climate model simulations. Dots represent the correlation between each
 128 regional reconstruction (see legend for region-colour) and the simulation averaged over the
 129 corresponding domain. Filled (unfilled) circles stand for significant (non-significant)
 130 correlation values. b) As in a), but for the single model ensembles; individual ensemble
 131 member correlations are shown in grey and the ensemble average in colour.

132

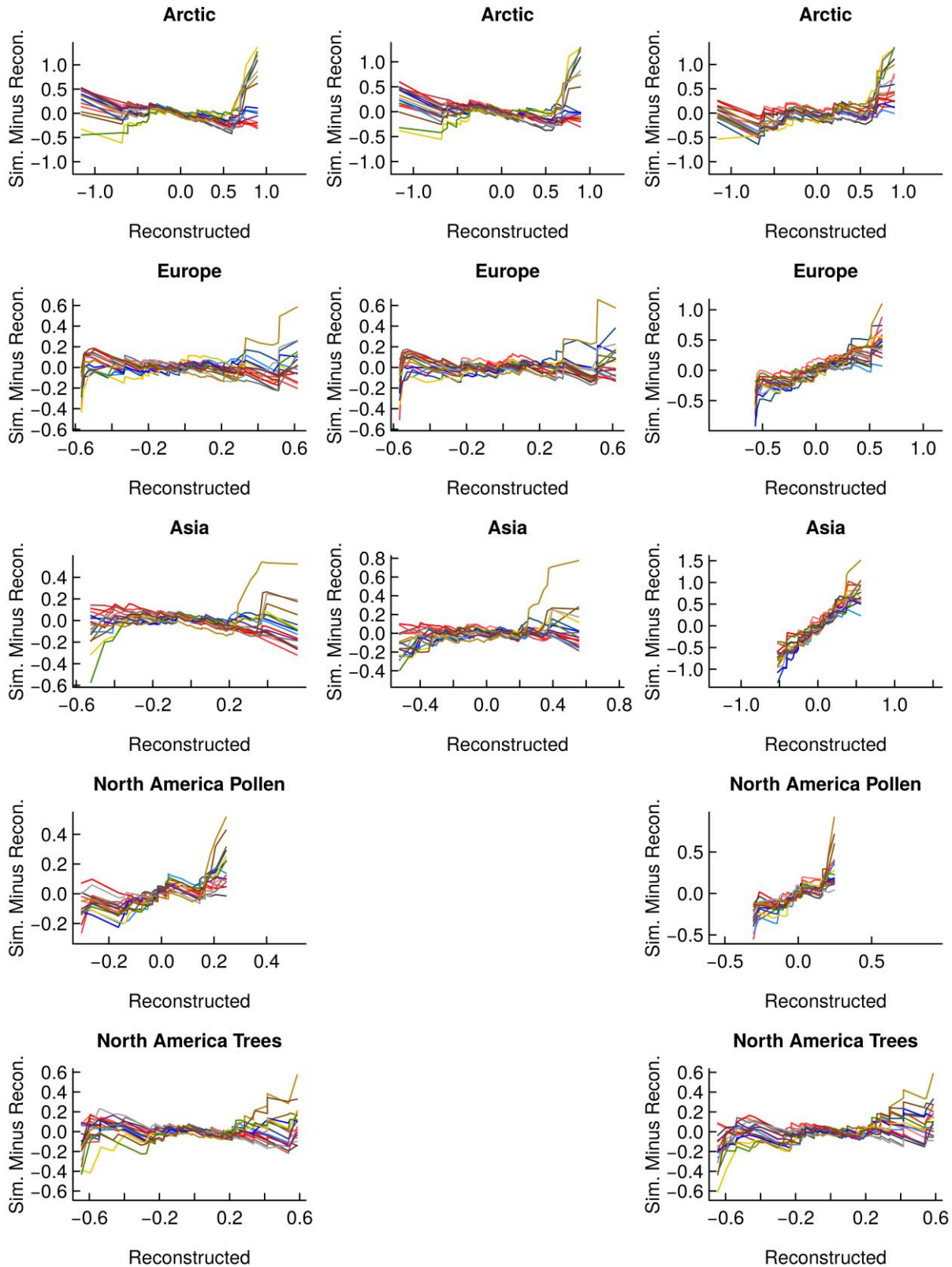


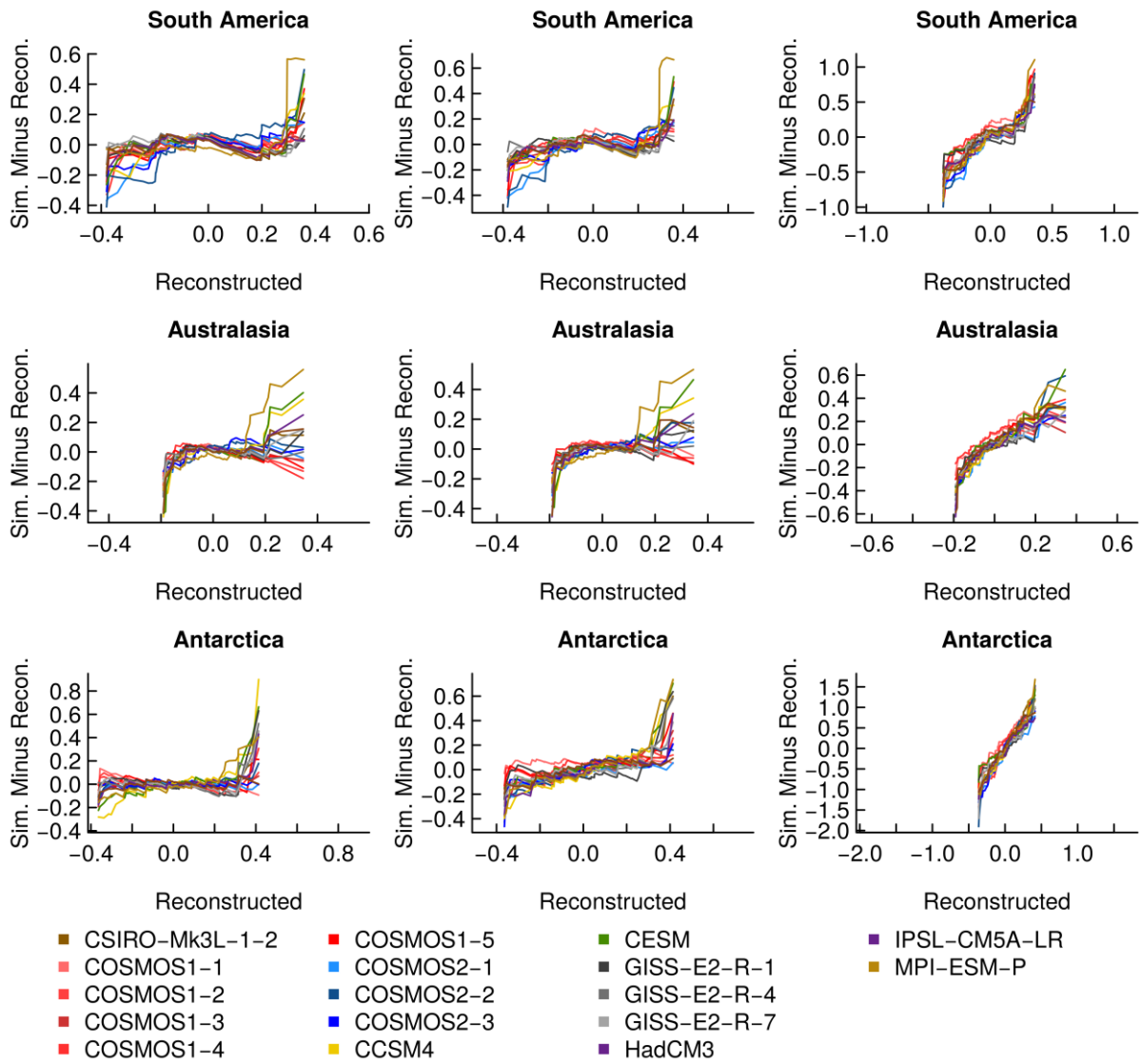
134

135 Figure S2. Normalized spectra of pre-PMIP3 (dashed) and PMIP3 (solid) simulations (grey)
 136 and reconstructions (red) for six PAGES 2k regional reconstructions for the period 850 to
 137 2000 CE. The spectra were computed from the normalized reconstructed and simulated
 138 regional temperatures using a 100 years Tukey-Hanning filter (Priestley, 1982). The
 139 simulations using solar forcing with higher (lower) variability are also highlighted in dark
 140 (light) grey.

141

142

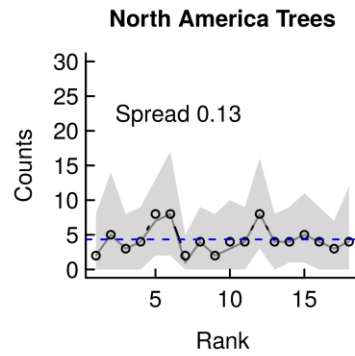
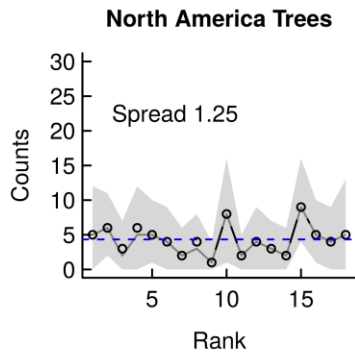
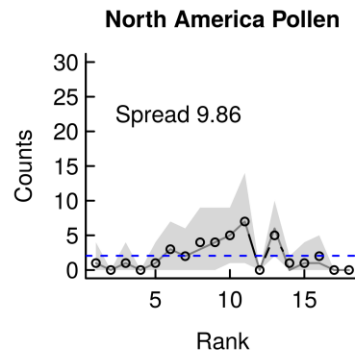
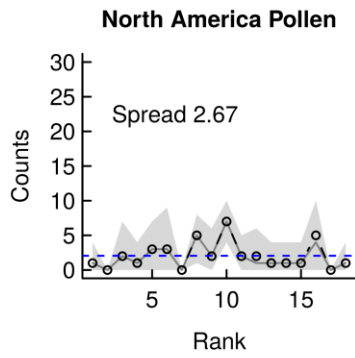
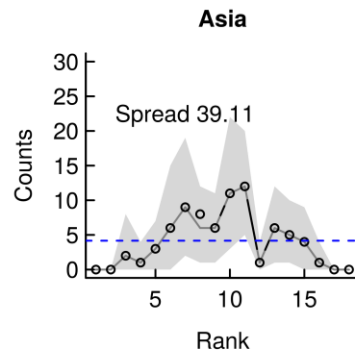
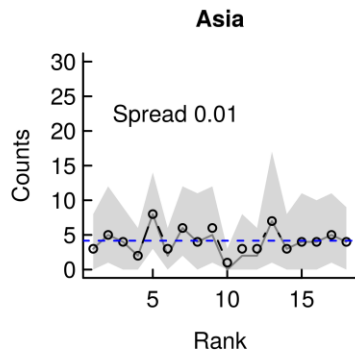
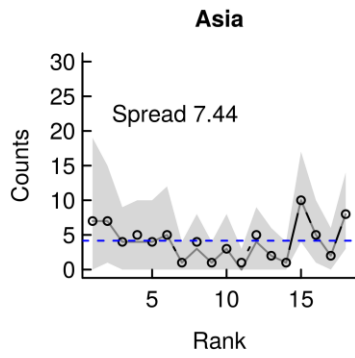
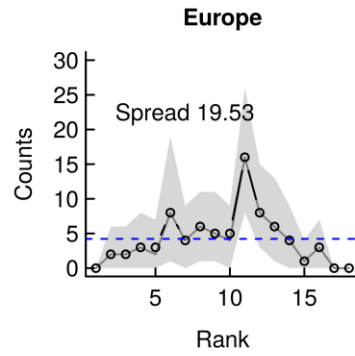
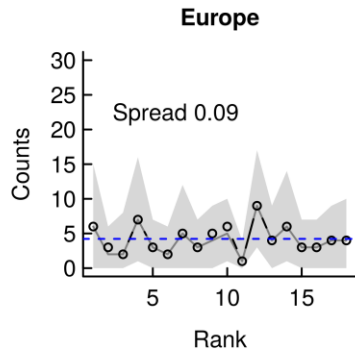
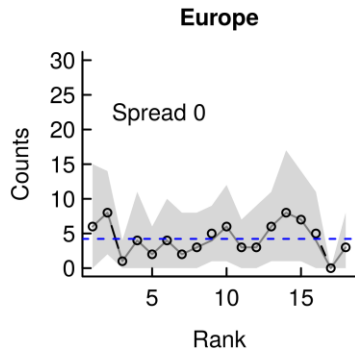
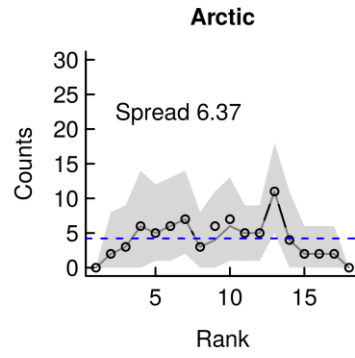
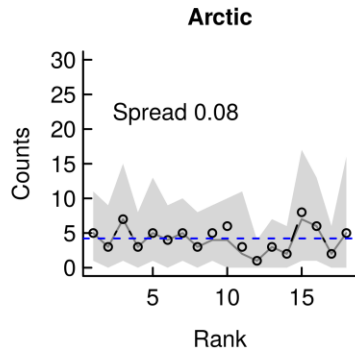
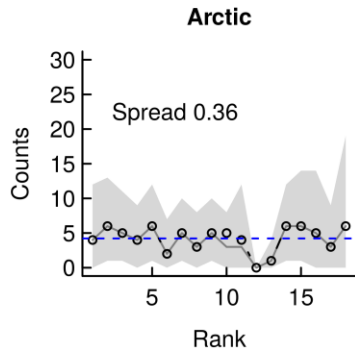


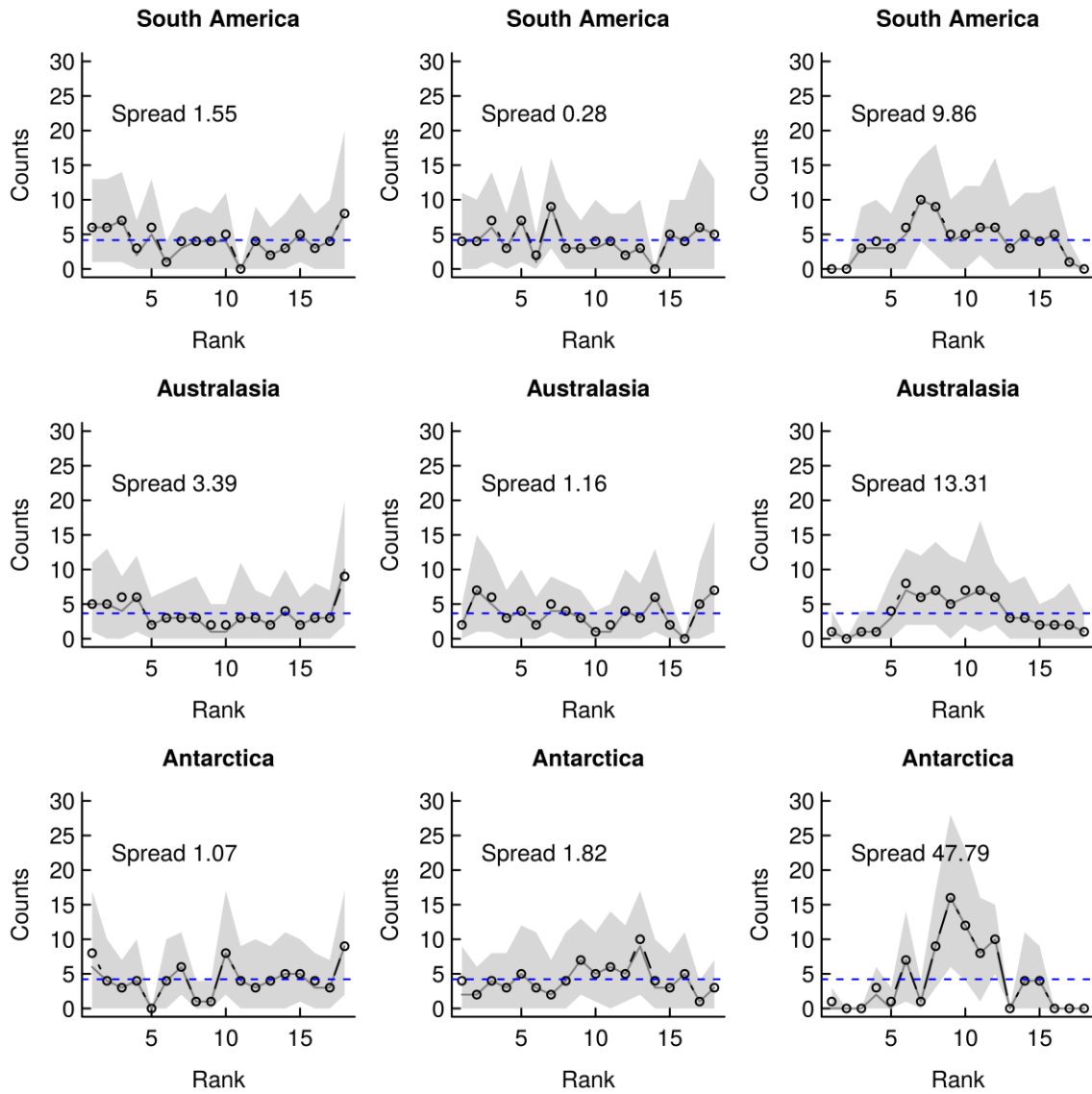


144

145 Figure S3. Climatological consistency: residual quantile-quantile plots for the full period for
 146 all the regions. In the left column, the uncertainty is neglected in the computations, in the
 147 middle column the original uncertainty divided by a factor $\sqrt{15}$ is used to take into account
 148 the smoothing while the original uncertainty is applied for the right column. There is no
 149 middle column for North American reconstructions because of their resolution.

150

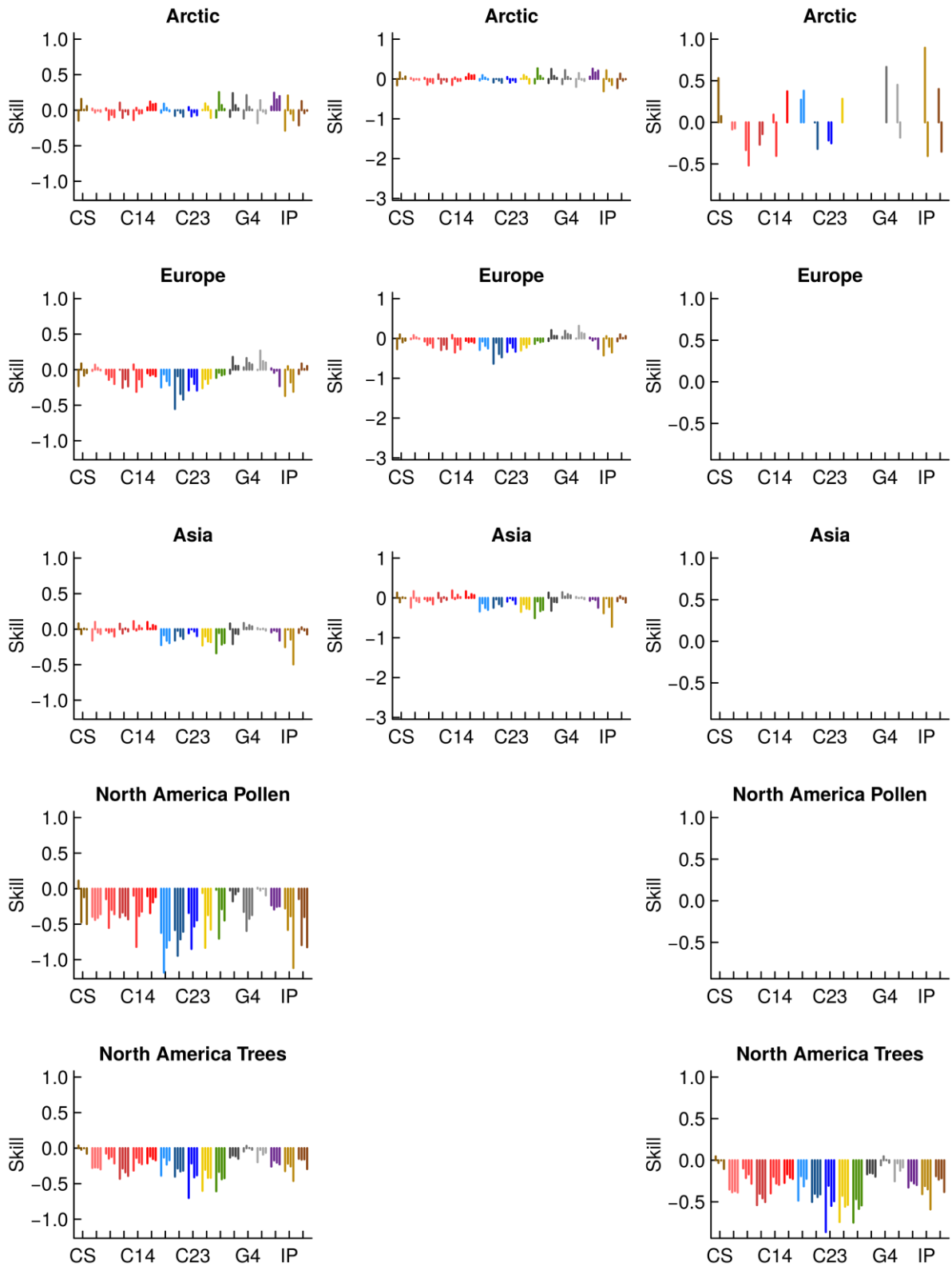


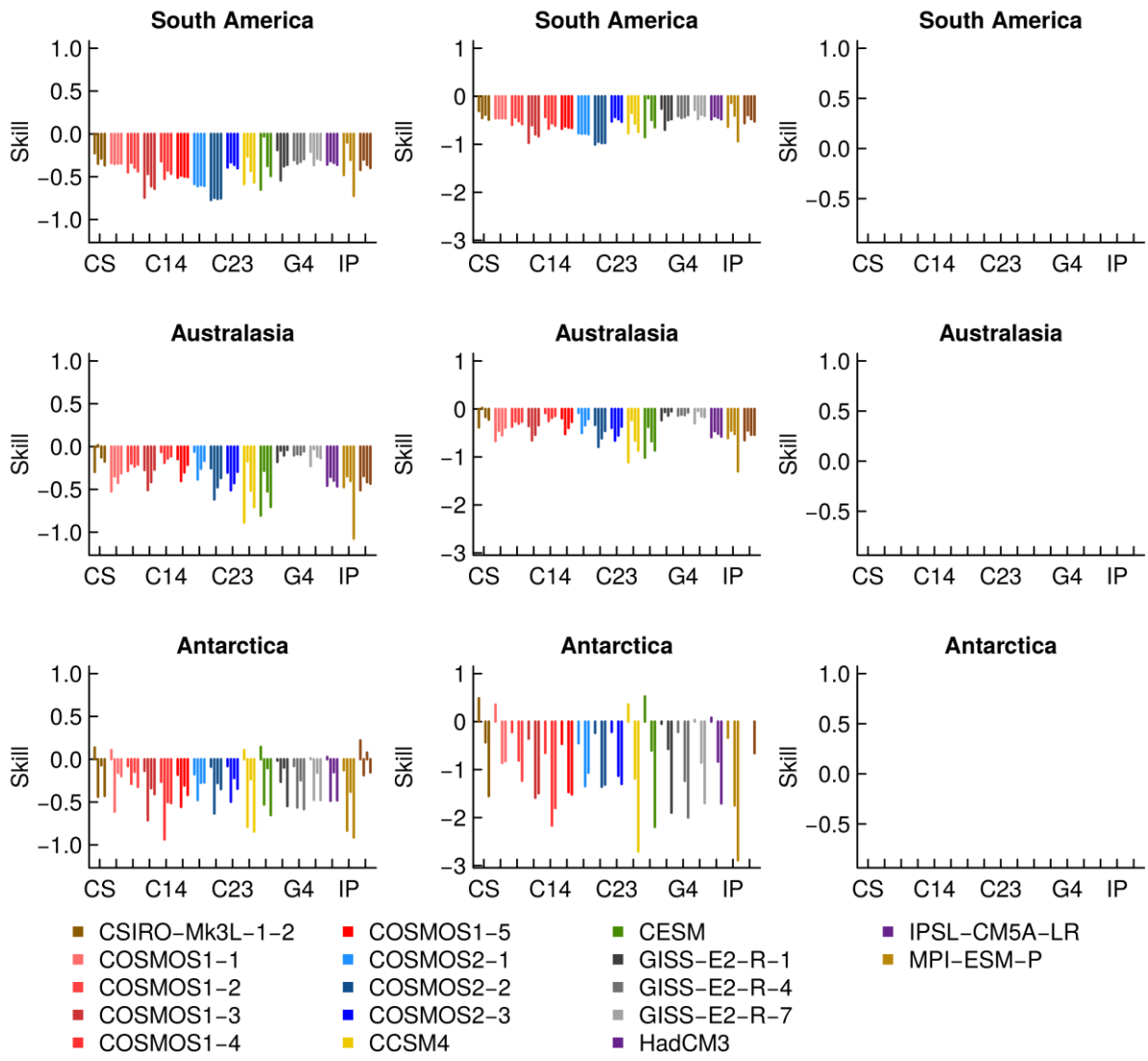


152

153 Figure S4. Probabilistic consistency for all the regions. The χ^2 goodness-of-fit statistic is
 154 applied to evaluate the consistency between observed rank count and the flat null hypothesis.
 155 The statistic can be decomposed to test for individual deviations like bias or spread (Jolliffe
 156 and Primo, 2008), as in Bothe et al. (2013a, b). In the left column, the uncertainty is neglected
 157 in the computations, in the middle column the original uncertainty divided by a factor $\sqrt{15}$ is
 158 used to take into account the smoothing while the original uncertainty is applied for the right
 159 column. There is no middle column for North American reconstructions because of their
 160 resolution.

161



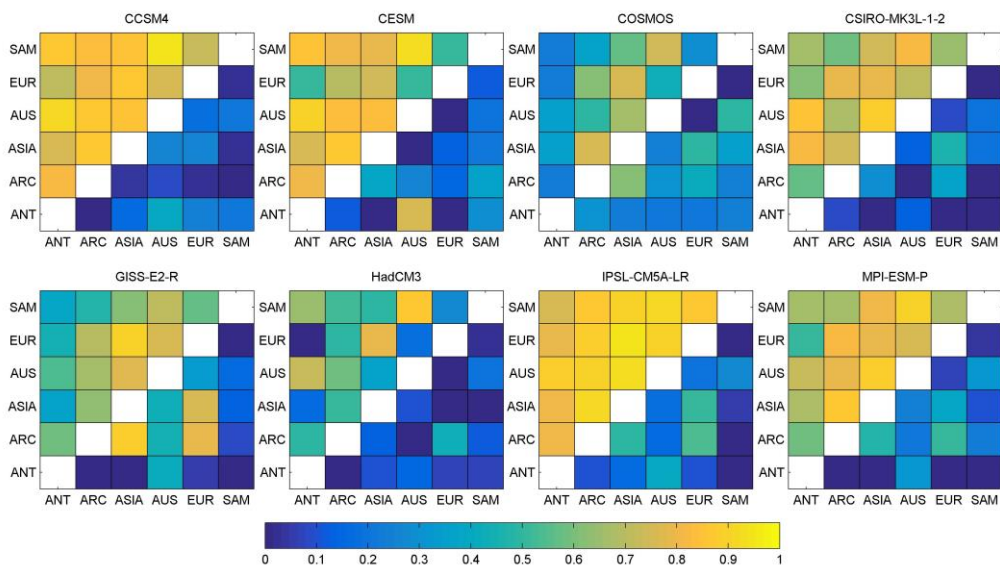


163

164 Figure S5. Skill metric for the individual models for all periods (bars from left to right: 850-
 165 1350, 1350-1850, 850-1850, 850-2000 CE). In the left column, the uncertainty is neglected in
 166 the computations, in the middle column the original uncertainty divided by a factor $\sqrt{15}$ is
 167 used to take into account the smoothing while the original uncertainty is applied for the right
 168 column. There is no middle column for North American reconstructions because of their
 169 resolution. When the skill is undefined no bar is shown.

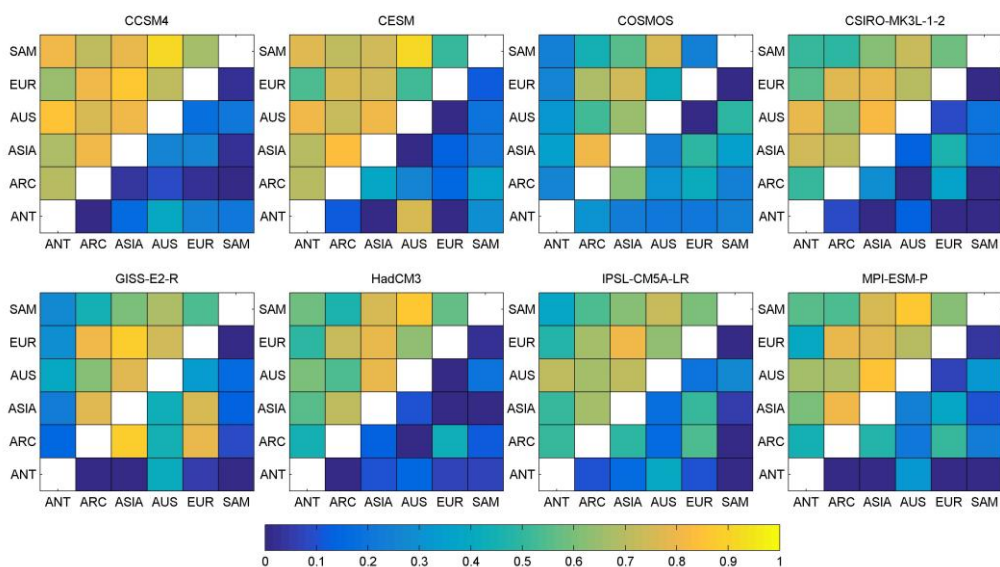
170

171 a) Correlation for the entire period



172

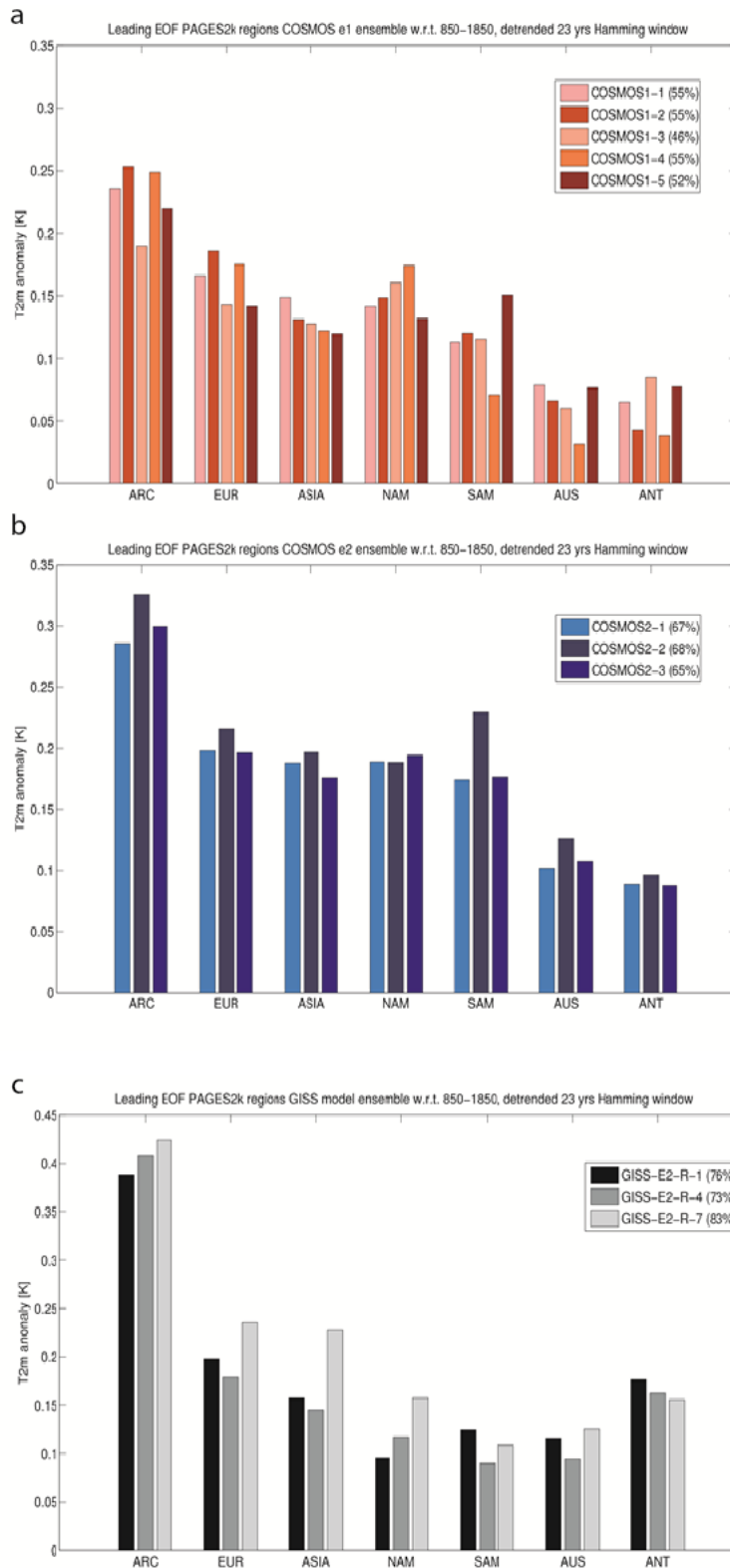
173 b) Correlation for the preindustrial period



174

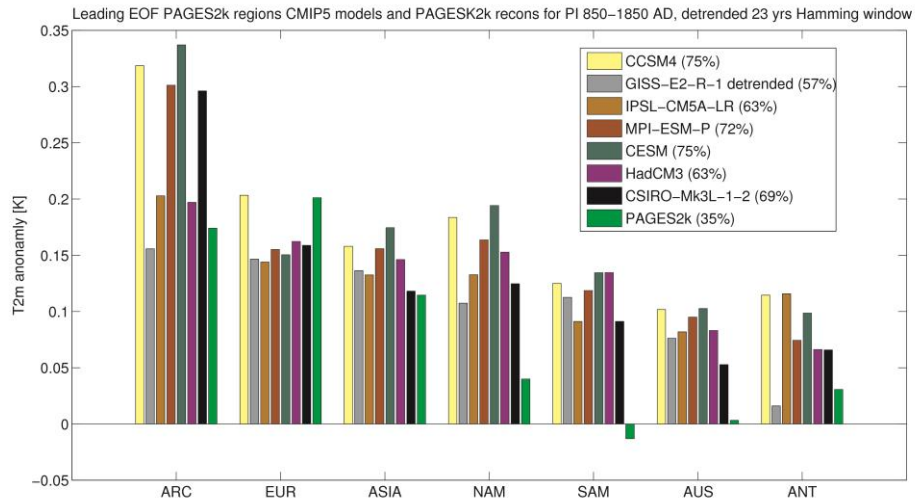
175 Figure S6. Correlations among the PAGES 2k regions for the different models using
176 detrended time series filtered with a 23-year Hamming filter. a) full period 1012 CE – 1978
177 CE, b) pre-industrial period 1012 CE -1850 CE. The upper left triangle represents the
178 correlations for the forced simulations while the lower right triangle represents the
179 correlations for the control runs (based on the full length of the control runs).

180



181
182
183
184
185
186
187

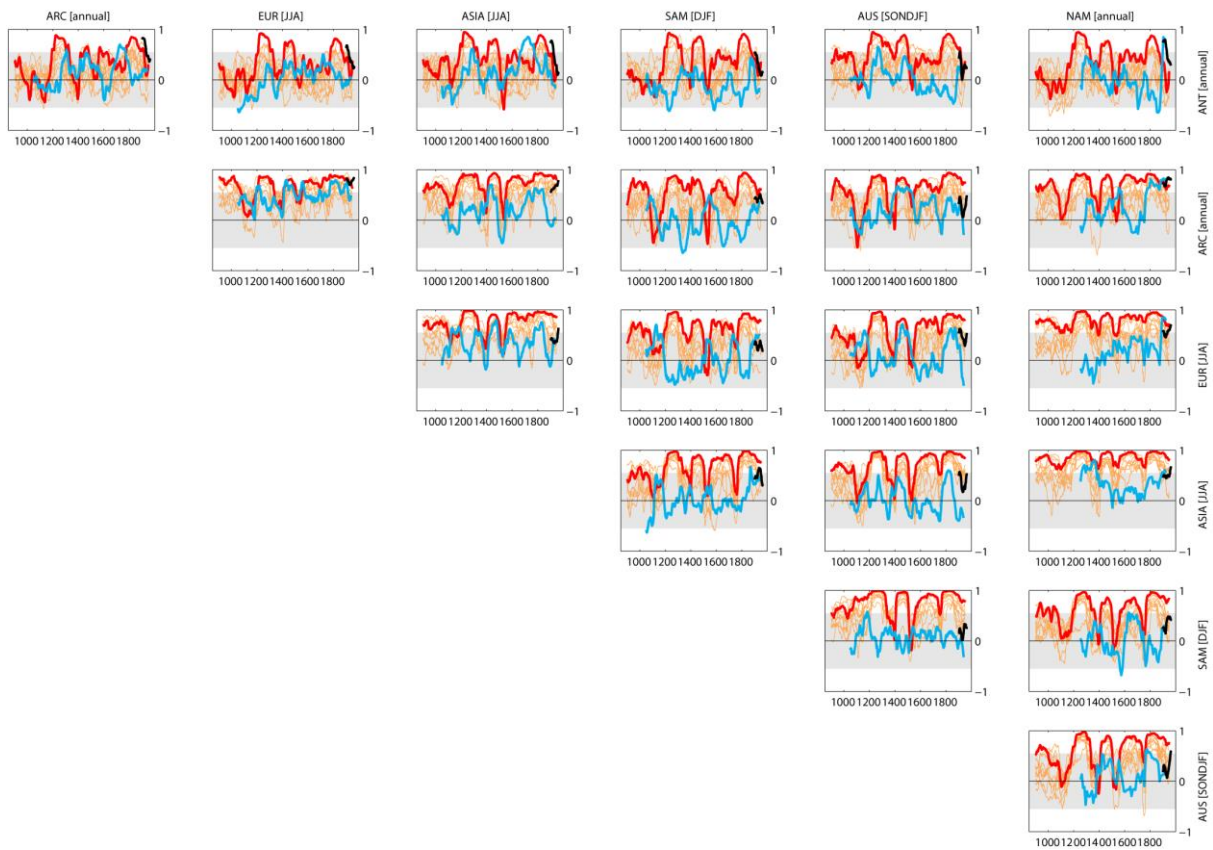
Figure S7. Same as Figure 6a for the leading EOF of the COSMOS ensemble with low (a) and high (b) solar activity changes and the GISS ensemble (c) models over the period 850–2004 AD. The eigenvectors are based on the covariance matrix with respect to temperature anomalies for the period 850–1850. The time series were filtered with a 23-year Hamming filter and were linearly detrended afterwards.



188
 189
 190
 191
 192
 193
 194

Figure S8. EOFs of the near-surface temperature simulated by each CMIP5/PMIP3 model and in reconstructions over the period 850–1850 CE. The time series were filtered with a 23-year Hamming filter and were linearly detrended before the covariance matrix was calculated.

195



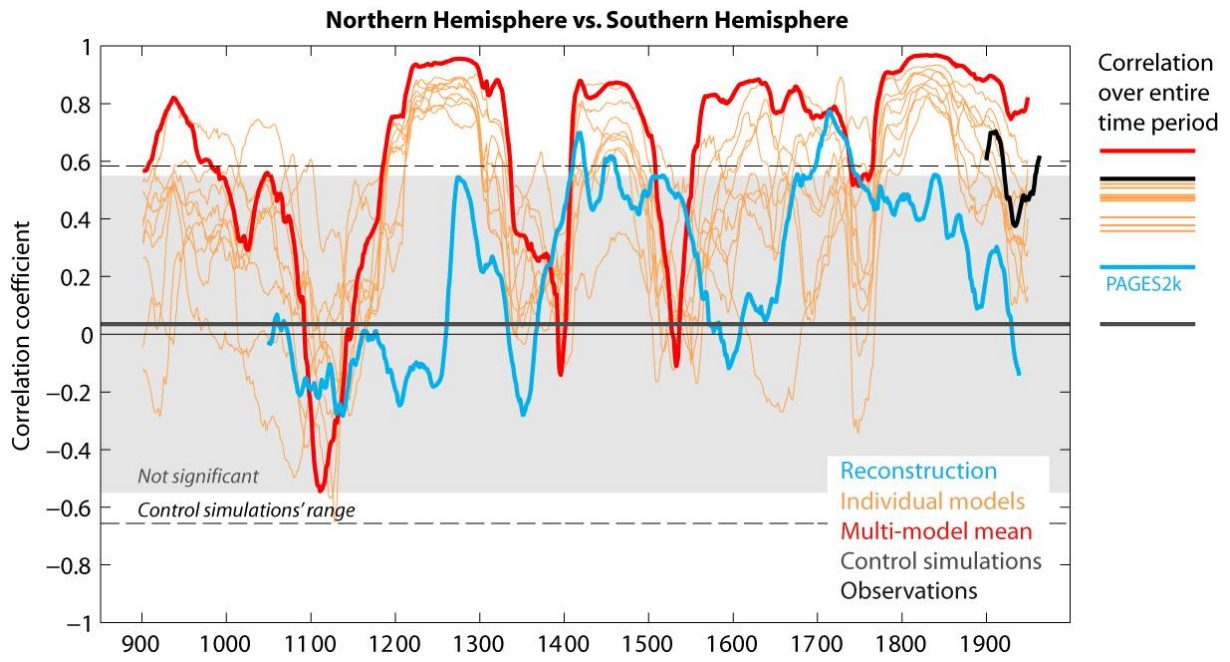
196

197

198 Figure S9. 100-year moving Tukey window correlations between all PAGES 2k regions for
199 the PAGES 2K reconstructions (blue) and PMIP3 models (8 models in orange, multi-model
200 mean in red) and observations from HadCRUT4 (black). Each 100-year segment is linearly
201 detrended beforehand. Grey shading illustrates not significant correlation at the 5% level.

202

203



204

205

206 Figure S10. 100-year moving Tukey window correlations between hemispheric averages for
 207 the PAGES 2k reconstructions (blue) and PMIP3 models (8 models in orange, multi-model
 208 mean in red) and observations from HadCRUT4 (black). Each 100-year segment is linearly
 209 detrended beforehand. Grey shading illustrates not significant correlation at the 5% level.

210

211

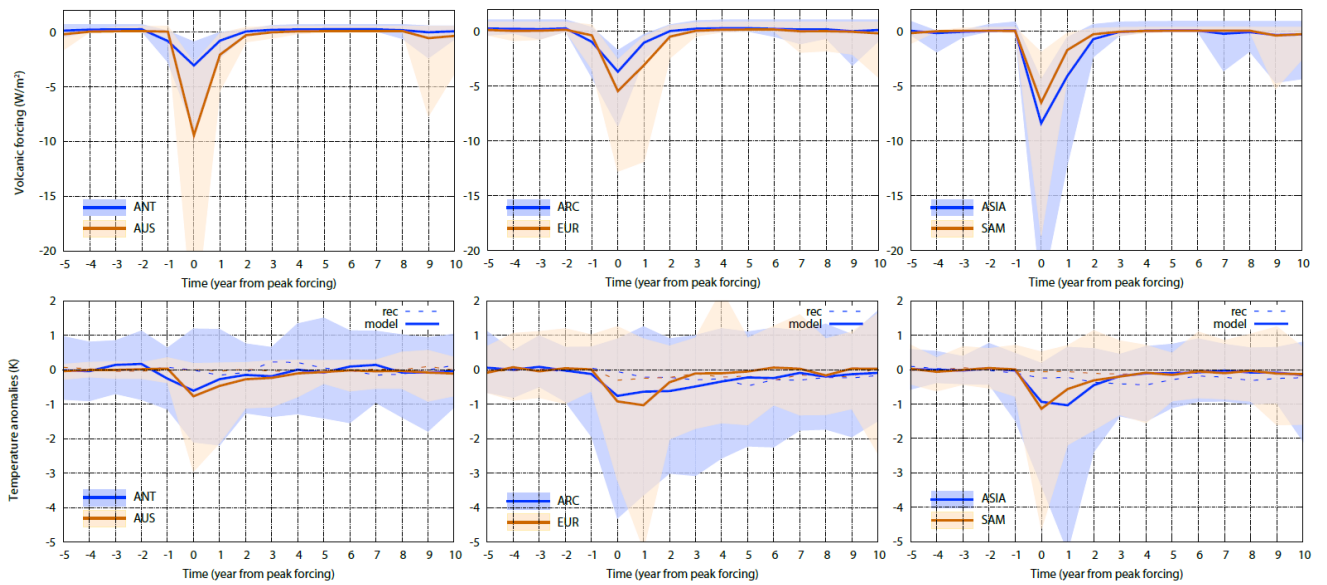


Figure S11. Same as Figure 8 but for the events selected in the Gao et al. (2008) reconstruction.

212

213

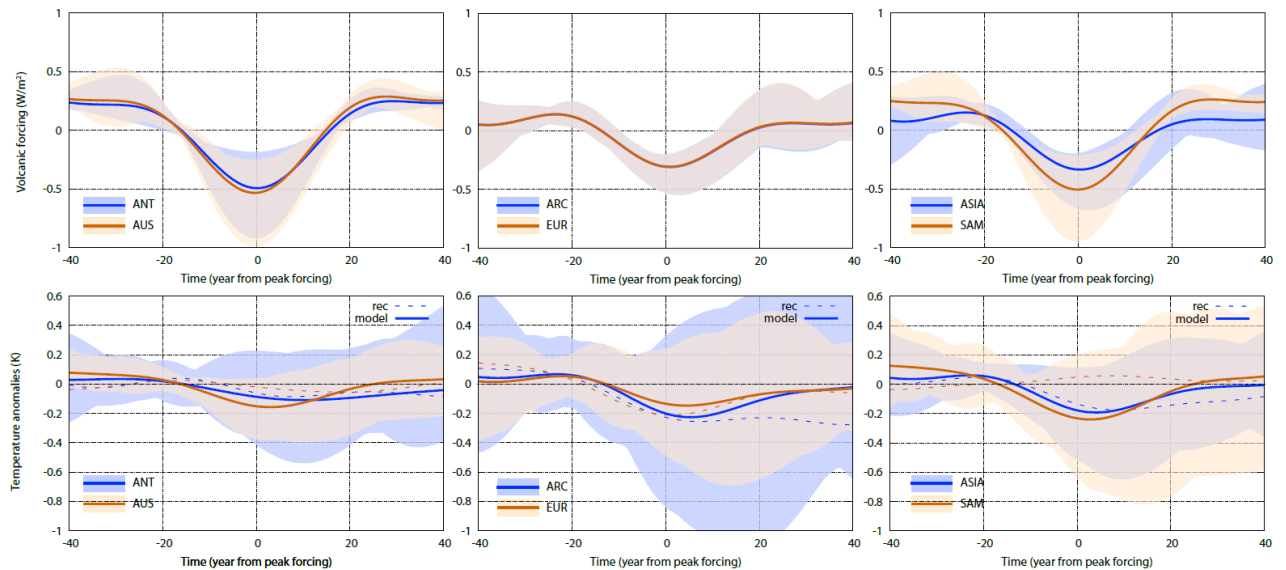


Figure S12. Superposed composites of volcanic forcing and temperature response during time intervals in which the years with peak negative forcing in the Crowley and Unterman (2012) reconstruction are aligned. The composite is produced by selecting the 5 strongest volcanic events, and a composite of the 30-year low pass filtered forcing and temperature series from 40 years before to 40 years after the date of the peak eruption. All the other elements are the same as in Figure 8.

214

215

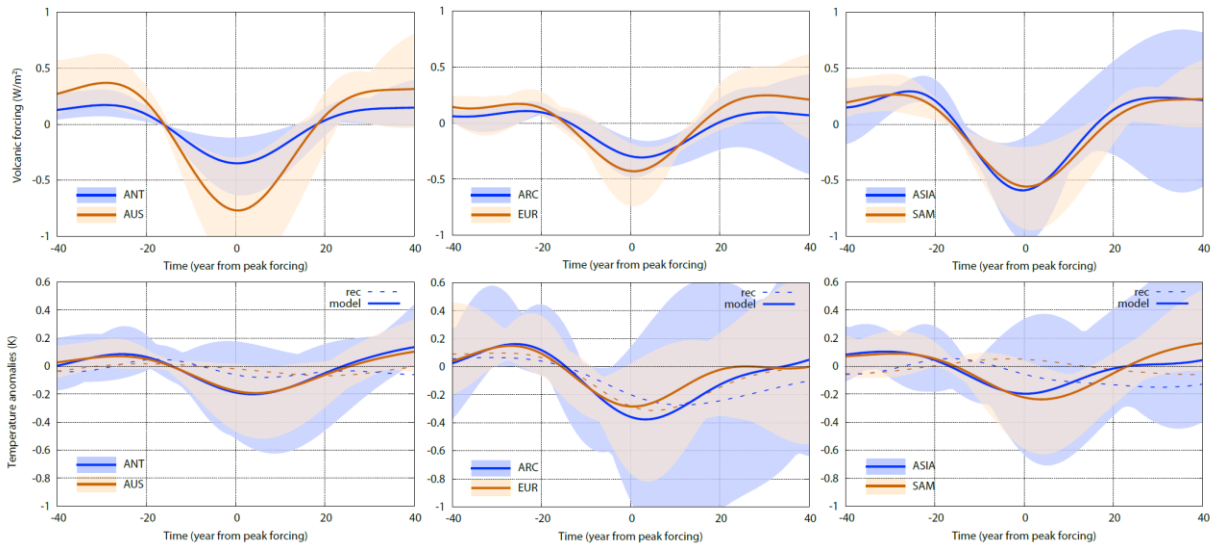


Figure S13. Same as Figure S12 but for the Gao et al. (2008) forcing.

216

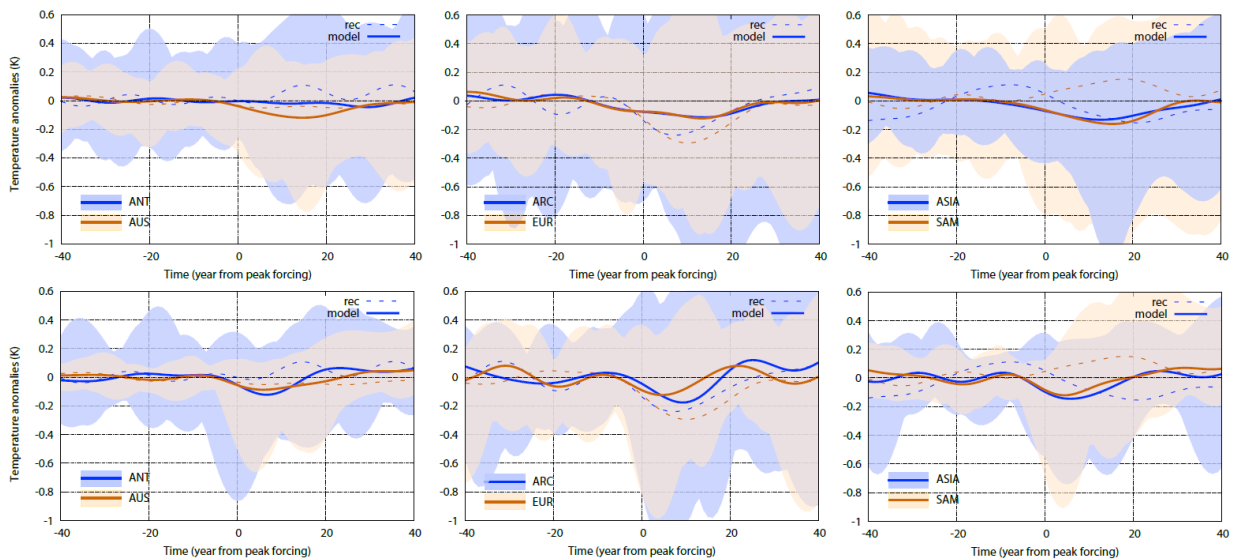
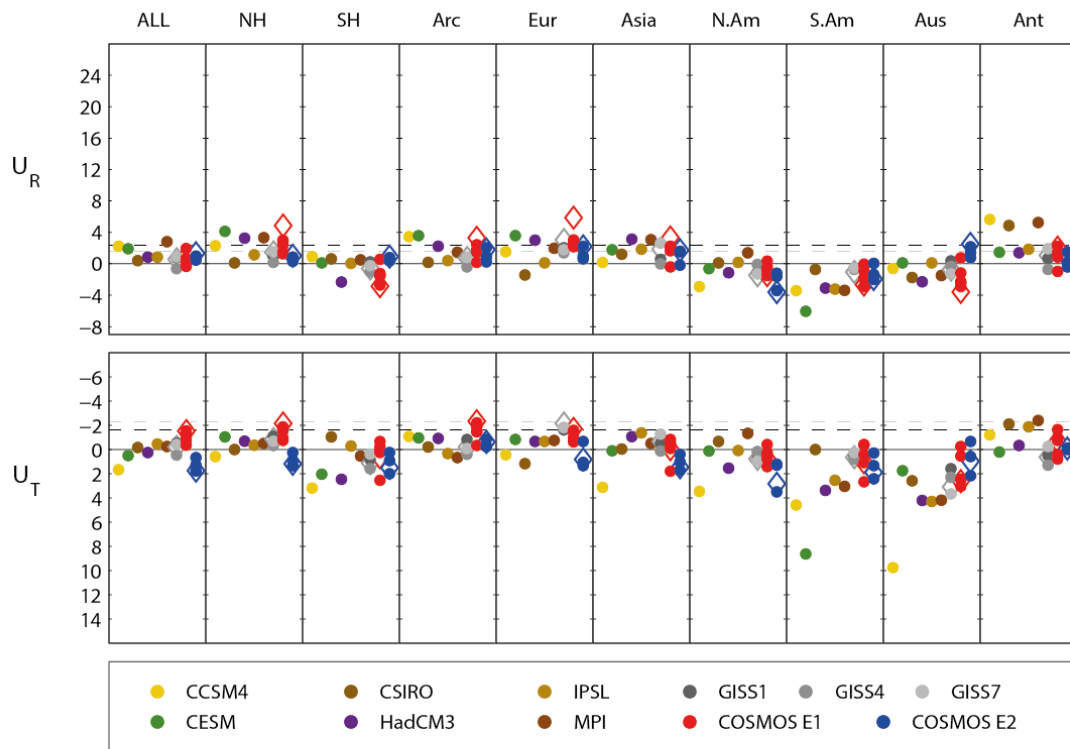


Figure S14. Superposed composites temperature response during selected periods in which the solar forcing was lowest (see text for details). Panels show results for reconstructions in six PAGES 2k regions and for model experiments performed using the volcanic forcing by: (top) the Crowley et al (2012); and (bottom) Gao et al. (2008). All the other elements are the same as in Figure 8.

217

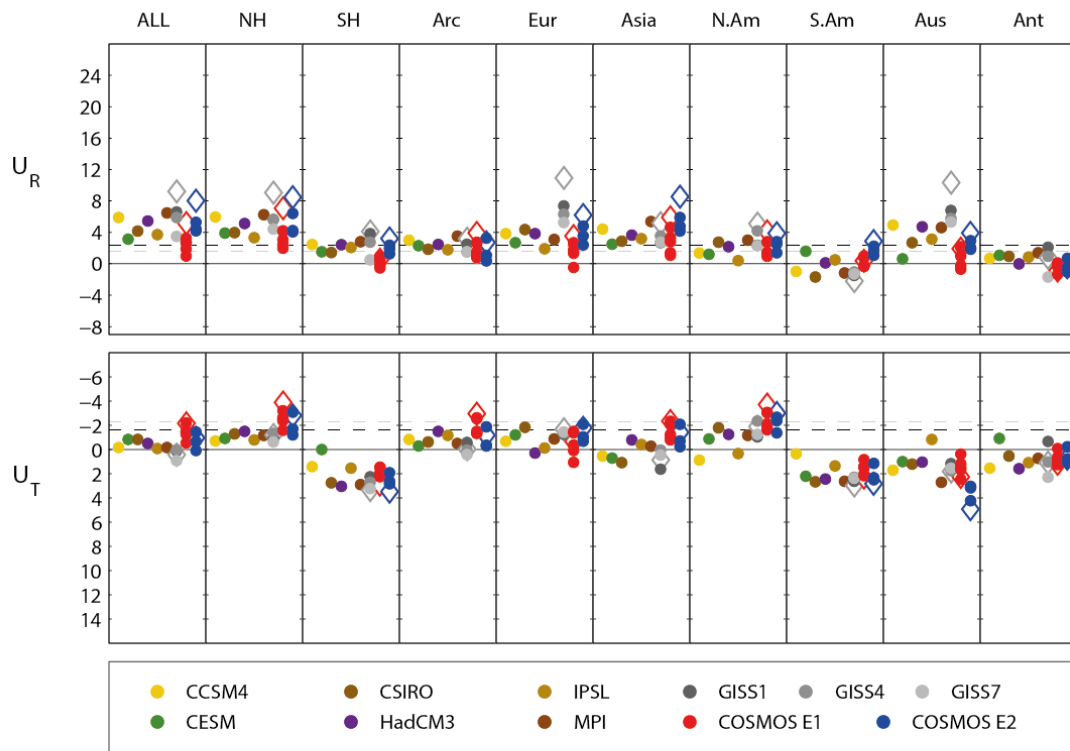
218



219

220 Figure S15: U_R and U_T statistics for PAGES 2k regions in the period 856–1350. Coloured
 221 dots: individual simulations. Diamonds: ensemble-mean results for COSMOS and GISS
 222 models. Positive U_R indicates that simulations and reconstructions share an effect of temporal
 223 changes in external forcings. Negative U_T indicates that a forced simulation is closer to the
 224 observed temperature variations than its own control simulation. Dashed lines show one-sided
 225 5% and 1% significance levels. Note the reversed vertical axis in the U_T graphs.

226

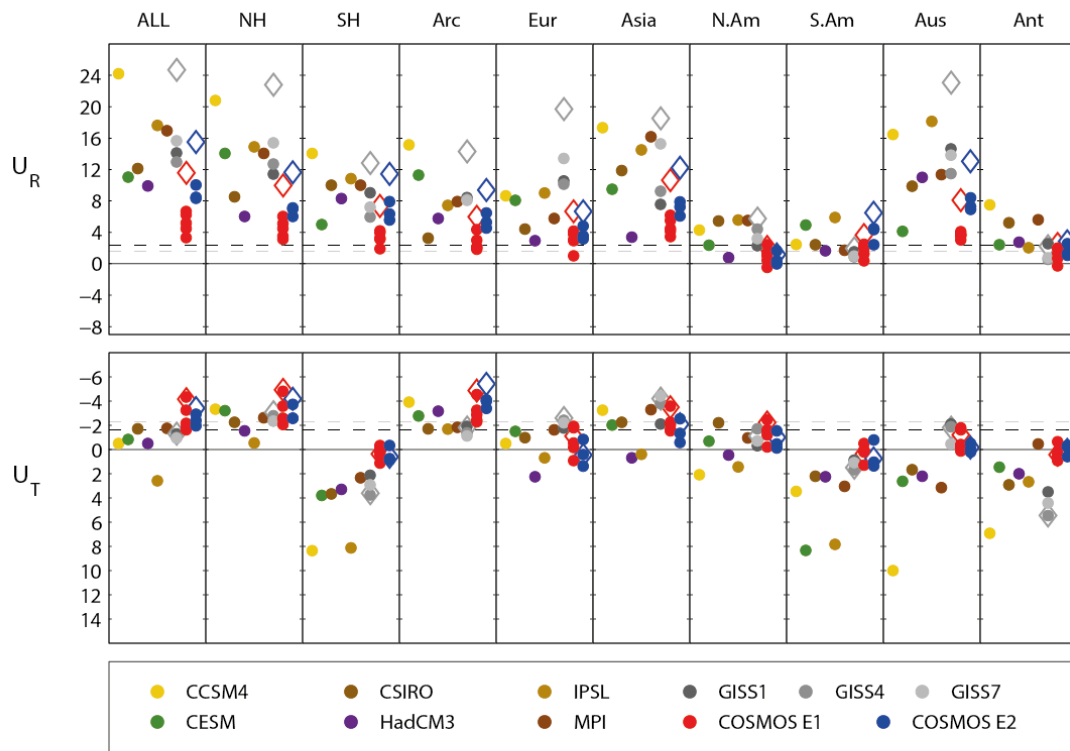


227

228 Figure S16: Same as Figure S15 but for the period 1356–1850.

229

230

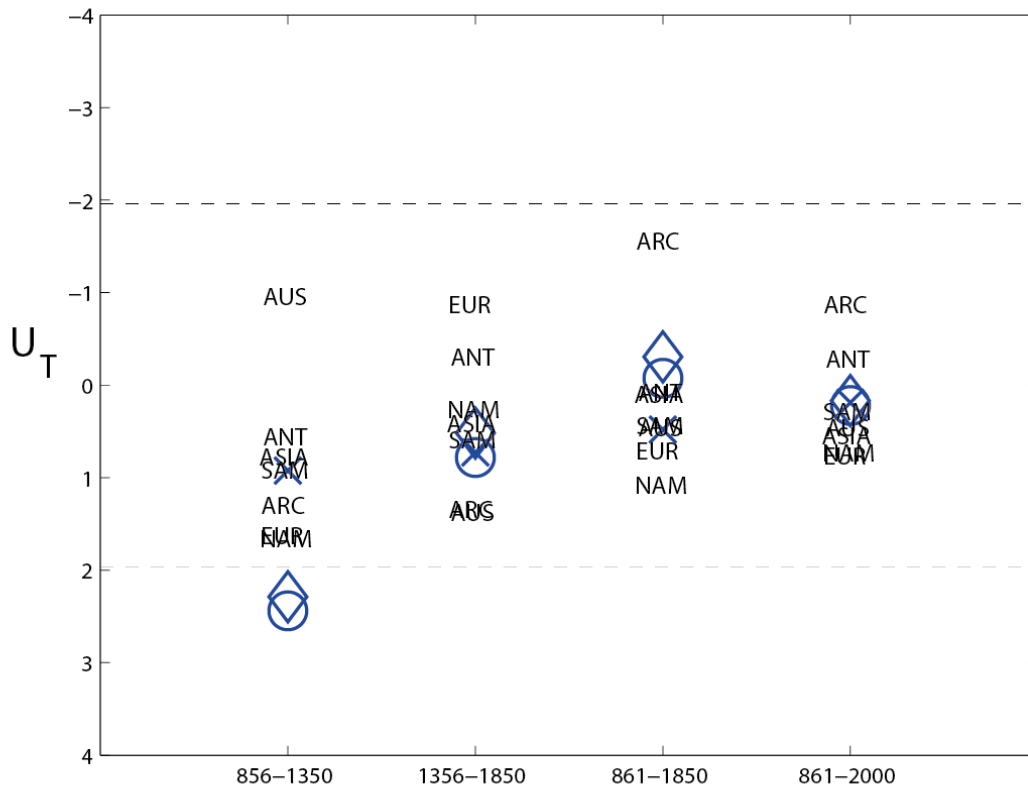


231

232 Figure S17: Same as Figure S15 but for the period 861–2000.

233

234



235

236 Figure S18: U_T statistics computed for a direct comparison between the high vs. low solar
 237 COSMOS simulation ensembles, using the method of Moberg et al. (2015, Appendix B4), for
 238 four different analysis periods. A negative U_T indicates that the high solar simulation
 239 ensemble is closer to the observed temperature variations than the low solar ensemble.
 240 Dashed lines show two-sided 5% significance levels for the null hypothesis that the two
 241 simulations are equivalent. Results for each region are indicated with their abbreviated names.
 242 Results where regions are combined are shown with blue symbols: All regions (circle),
 243 Northern Hemisphere regions (diamond), Southern Hemisphere regions (cross).